# Ionization of Linear Alcohols by Strong Optical Fields†

**D. Mathur,‡,§ T. Hatamoto,‡ M. Okunishi,‡ G. Prümper,‡ T. Lischke,‡ K. Shimada,‡ and K. Ueda‡**

*Institute of Multidisciplinary Research for Advanced Materials, Tohoku University, Sendai 980-8577, Japan, and Tata Institute of Fundamental Research, 1 Homi Bhabha Road, Mumbai 400 005, India*

*Received: April 24, 2007; In Final Form: July 30, 2007*

We have experimentally probed the strong-field ionization dynamics of gas-phase linear alcohols, methanol, ethanol, and 1-propanol, by irradiating them with intense, femtosecond-duration laser pulses of 800 and 400 nm wavelength. Specifically, we make high resolution measurements of the energies of electrons that are ionized by the action of the optical field. Our electron spectroscopy measurements enable us to bifurcate the dynamics into multiphoton ionization and tunneling ionization regimes. In the case of 800 nm irradiation, such bifurcation into different ionization regimes is reasonably rationalized within the framework of the adiabaticity parameter based on the original Keldysh−Faisal−Reiss model of atomic ionization, without recourse to any structure-dependent modifications to the theory. In that sense, our 800 nm spectroscopy indicates that the linear alcohols exhibit atom-like properties as far as strong field ionization dynamics in the multiphoton ionization and tunneling regimes are concerned. We also explore the limitations of this atom-like picture by making measurements with 400 nm photons wherein the ponderomotive potential experienced by the ionized electrons is much less than the photon energy; effects that are purely molecular then appear to influence the strong field dynamics.

## Introduction

Femtosecond lasers are now commercially available that enable focused intensities in the TW $cm^{-2}$ to PW $cm^{-2}$ range to be readily achieved in tabletop systems. Such intensities give rise to optical fields whose magnitudes match the Coulombic fields that exist within individual atoms, molecules, and clusters. Irradiation of these species by such strong optical fields inevitably leads to ionization; the dynamics are highly nonlinear and theoretical treatments have to be nonperturbative. There has been burgeoning interest in strong field molecular dynamics in the course of the past decade or so but the focus of experimental attention has mainly been directed toward studying the positively charged ions that are produced in the course of the field−molecule interaction.[1−12] We report here the results of a careful experimental study of energy spectra of electrons that are ejected when a series of linear alcohol molecules in the gas phase, methanol, ethanol, and 1-propanol, are ionized using 100−150 fs-long pulses of intense light of either 800 or 400 nm wavelength.

Our experiments were conducted with the aim of utilizing high-resolution electron spectroscopy to explore the extent to which oft-used models of atomic ionization in strong fields provide an adequate enough description of *molecular* ionization phenomena. Volkov's exact solution, in 1935, of the Dirac equation in the presence of a plane-wave field,[13] and subsequent pioneering work[14−18] carried out in the 1950s and 1960s, form the theoretical underpinnings of contemporary studies of molecular dynamics in strong fields, with the core of the subject relying on the theoretical treatment of electron dynamics in intense electromagnetic fields. Contemporary descriptions of how atoms ionize upon irradiation by strong optical fields rely on the Keldysh−Faisal−Reiss (KFR) model[19−21] in conjunction with a Coulomb correction[22] and the ADK (Ammosov−Delone−Krainov) tunneling theory.[23] The theoretical description of the interaction of the optical field with the irradiated atom is, in these models, approximated by a zero-range potential. In the case of multiatom species, however, the spatial extent of a molecule and, for most molecular species, the associated spatial anisotropy, imply that *atomic* descriptions of strong-field ionization might not be expected to prove adequate in properly accounting for measured ionization rates. Attempts have been made to modify the KFR and ADK models so as to take into account both the effects of molecular symmetry[24] and of the dynamic spatial alignment of molecules[25] that can be induced by linearly polarized optical pulses of sufficiently long duration. For a few molecules, notably diatomics like $N_2$, good agreement has been demonstrated between experimentally measured ionization rates and absolute ion yields that are predicted by both the KFR-ADK descriptions[26] and modified models.[27] Similar good agreement with atomic theories has also been demonstrated in measurements of absolute ion yields made in a series of amines.[28] Strong alignment effects in total ionization rates and electron angular distributions have been demonstrated in the results of calculations performed for polyatomic molecules, benzene, and ethylene[29] and have been interpreted in terms of the HOMO symmetry of these molecules. It is clear that electron delocalization needs to be properly accounted for to characterize light−matter interaction involving polyatomic molecules, and to this end an appropriately length-modified Keldysh parameter[30] has been invoked in efforts to delineate the relative importance of multiphoton ionization (MPI) and tunneling ionization in some aromatic molecules.

Electron ejection from an atom that is irradiated by strong laser fields is most frequently described in terms of either MPI

† Part of the "Sheng Hsien Lin Festschrift".
‡ Tohoku University.
§ Tata Institute of Fundamental Research.

10.1021/jp0731452 CCC: $37.00 
Published on Web 08/21/2007

or tunneling ionization, with the limit between the two given by the adiabaticity or Keldysh parameter, $\gamma$ [$=(I_e/2U_p)^{1/2}$], the ratio of the tunneling time to the optical period. In this expression for $\gamma$, $I_e$ denotes the atomic ionization energy and $U_p$ is the ponderomotive potential associated with the optical field. A range of $\gamma$-values can be readily obtained in an experiment by varying the laser intensity and/or the nature of the target that is being irradiated. It seems established that tunnel ionization dominates the ionization dynamics for small values of $\gamma$ ($<1$). Here, the shape of the electron energy spectrum is largely determined by the classical propagation of the electron in the optical field. For large values of $\gamma$ ($>1$), the multiphoton picture appears more appropriate in describing the ionization dynamics and, in such cases, atomic resonances and above-threshold ionization peaks manifest themselves in electron spectra.

Although a reasonably robust framework now exists within which to understand the ionization dynamics of atoms in the tunneling regime ($\gamma <1$), progress in the multiphoton regime ($\gamma >1$) has been less spectacular. Chaloupka et al.[31] reported the first electron−ion coincidence experiments that probed the transition from tunneling to multiphoton ionization in atomic double ionization: electron spectra in Xe showed well-resolved resonance-like structures whereas in Ar featureless spectra were obtained, indicative of electron rescattering. Details of the resonance-like peaks in the electron spectra remain to be understood, but sequential ionization seems to be the key process.

To deal with ionization dynamics in molecules, a simple recipe has been developed[30] that introduces a structure-based (length-based) $\gamma$-parameter that seeks to obviate any shortcomings of a zero-range potential. The recipe involves the following steps:

(i) An *ab initio* geometry optimization is first carried out for the neutral molecule in its electronic ground state.

(ii) Using this geometry, the wave function of the singly ionized molecule is computed.

(iii) Such a wave function is then used to derive an approximate rectangular potential well whose width corresponds to the distance between the classical turning points and whose depth is equivalent to the ionization energy of the neutral molecule.

(iv) The rectangular potential is modified by superimposition of an external static potential that approximates the optical field that the molecule is subjected to.

(v) The tunneling rate from this field-dressed potential is then deduced using the semiclassical Wentzel−Kramers−Brillouin (WKB) method. The resulting tunneling frequency is used to derive what is called a structure-modified Keldysh parameter.

To properly account for the role played by inner barriers that exist within realistic molecular potentials, the zero-range potential may be replaced by a Coulomb potential or, in the case of diatomics and some triatomics, by a quantumchemically computed *ab initio* molecular potential.

On the basis of applying the length-based $\gamma$ to aromatics like benzene, naphthalene, and anthracene, Levis and co-workers have concluded[30] that tunnel ionization occurs at much lower optical fields for molecules with extended electronic orbitals than for atoms of similar ionization energy. However, other experiments on large polyatomics, initially conducted by Corkum, Stolow, and co-workers,[31,32] yielded results that suggested the opposite: it is more difficult to tunnel ionize some polyatomics than atoms that possess similar values of ionization energy. The field-induced polarization of delocalized electrons within such polyatomics, with its resultant dynamic shielding effect, contributes additively to the potential barrier, making the active electron's escape by tunneling through the barrier more difficult, resulting in distinctly higher thresholds for tunnel ionization.[33]

Lezius et al.[34] have ascribed the difficulty of properly accounting for molecular ionization dynamics in strong optical fields not only to the inadequacies of the zero-range potential that is inherent to atomic theories but also to the fact that atomic approaches rely on a "single active electron" picture within which no account can be taken of any electron dynamics within the molecular potential. It has been pointed out[33] that the limit $\gamma < 1$ that defines the tunneling regime does not identify the adiabaticity of the electronic response of a molecule; it relates only to the tunneling of a single electron through the potential barrier.

The molecular experiments that we report here were conducted using alcohol molecules, typical of linear molecules comprising C−H, C−O, and O−H bonds. Electrons associated with C−H bonds are relatively unpolarizable. Regarding alcohol molecules as alkyl derivates of water, we take our cue from the electronic structure of the ground state of $H_2O$: $(1a_1)^2(2a_1)^2(1b_2)^2(3a_1)^2(1b_1)$.[2] The highest occupied water orbital, $1b_1$, is nonbonding in character, almost a nearly pure 2p atomic orbital on oxygen and oriented perpendicular to the molecular plane. In the case of alcohols, the highest occupied orbital (where it is denoted $n_0$) retains its nonbonding character but is somewhat more mixed with the $\pi$-orbitals of the alkyl group. From the perspective of probing the efficacy, or otherwise, of the KFR-ADK picture in accounting for strong-field molecular ionization dynamics, it is pertinent to note that there is nothing "special" about the alcohol molecules we have studied; we regard them simply as archetypal linear polyatomics of modest dimensions. A subset of our electron spectroscopy results from experiments conducted using only 800 nm light has been reported in a preliminary communication[35] and revealed, somewhat unexpectedly, that rationalization of the electron ionization dynamics in terms of the MPI and tunneling regimes could be readily accomplished using the conventional (unmodified) Keldysh parameter, indicating that the linear alcohols behave in atom-like manner, albeit an atom with an extended spatial extent. Furthermore, these 800 nm experiments also indicated that the length-modified Keldysh parameter may not be a useful quantity to describe the transition from the MPI to the tunnel ionization regime. To probe the limitations of the atom-like picture of strong field ionization dynamics of the linear alcohols, we have extended our previous measurements by also conducting experiments using 400 nm photons. Access to the regime wherein the ponderomotive potential is less than the energy of a single photon helps us probe the purely *molecular* facets of the strong field dynamics for these molecules and provides data that can be used as a benchmark to evaluate the extent of validity of an atom-like picture of strong field ionization of linear alcohols.[35]

## Experimental Apparatus

We used a regeneratively amplified Ti:sapphire laser system (pulse width:100 fs, repetition rate: 1 kHz) to obtain 800 nm laser light; 400 nm laser pulses were generated by us using a BBO crystal. The pulse duration of the 400 nm laser light, as estimated from the power spectrum of the laser beam measured by a grating spectrometer, was typically 100 fs. We used neutral-density filters to control the pulse intensity and a half-wave plate to control the direction of the linear polarization of the laser light. Evaporated alcohol molecules were introduced into our

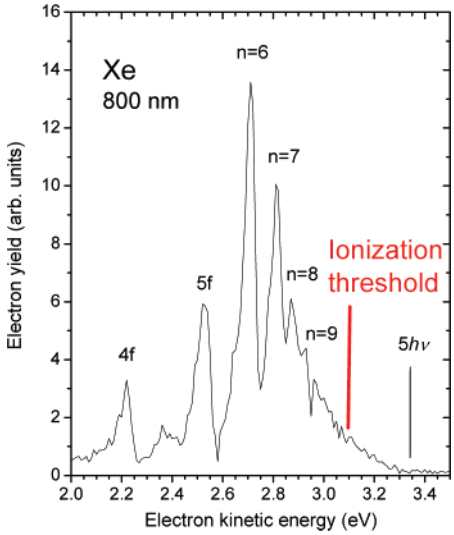


**Figure 1.** Photoelectron spectrum of Xe measured using 800 nm pulses of 100 fs duration, with a peak intensity of 100 TW cm$^{-2}$. Note the well-resolved Rydberg progression converging on the $^2P_{3/2}$ threshold of $Xe^+$. Such spectra were used to calibrate the energy scale in the electron spectra reported here (see text).

vacuum chamber effusively through a grounded copper needle. The needle tip was kept 10 mm away from the laser focus spot to avoid the signals originating from electrons colliding with the needle. The vacuum chamber was evacuated by a turbo molecular pump to a base pressure of $2 \times 10^{-9}$ Torr; typical operating pressures were maintained between $2 \times 10^{-8}$ and $1 \times 10^{-6}$ Torr.

The laser beam entered the vacuum chamber through a quartz window and was focused by a concave mirror ($f = 60$ mm) so as to achieve peak intensities in the $10^{12}$ to $10^{14}$ W cm$^{-2}$ range so as to cover a fairly wide range of $\gamma$-values. The kinetic energy distribution of ionized electrons was determined using a linear time-of-flight spectrometer of 264 mm long. Laser interaction and drift regions were both kept field free. The electrons were detected by a microchannel plate (MCP) detector. The electron kinetic energies were determined from their times-of-flight (TOF): the start signal for the TOF measurement was derived from a photodiode reacting to the laser pulse and the stop signal was from the electron pulse via a constant fraction discriminator.

The absolute values of peak laser intensity were estimated by separate photoelectron measurements of Xe atoms. A proper measure of the energy scale is an important facet of electron spectroscopy. Our energy scale calibration was also with reference to MPI of Xe. A typical photoelectron spectrum that we measured at $1 \times 10^{14}$ W cm$^{-2}$ peak intensity using 400 nm light is depicted in Figure 1. The high-resolution capability of our spectrometer ($E/\Delta E > 50$) is demonstrated by the observed Rydberg structure (Freeman resonances),[24] with levels converging on $^2P_{3/2}$ $Xe^+$ ionization threshold at 12.13 eV. The Stark energy shifts of the photoelectron peaks due to the electron ponderomotive potential were measured as a function of incident laser power. Because the energy shifts are proportional to the peak laser intensity, the measured energy shifts, which were associated with laser power readings, directly yielded absolute values of the peak laser intensity at the ionization point, without recourse to direct measurement of the focused laser spot size. For 800 nm laser irradiation, the absolute values of the peak laser intensity at the ionization point were also obtained from the ratio of $Xe^{++}/Xe^+$ measured as a function of the incident laser power; we used the results of Talebpour et al.[36] as reference data. The consistent results from these two different approaches confirmed the accuracy of our measurement for the peak laser intensity.

## Results and Discussion

**General Features of the Spectra.** Typical electron spectra measured when methanol, ethanol, and 1-propanol molecules are irradiated by 800 and 400 nm light are depicted in Figures 2−4. To make these measurements the peak value of the intensity was varied over the range 12−168 TW cm$^{-2}$, covering a range of $\gamma$-values from ~6 to 0.8 (see Table 1), where $\gamma$ is the conventional (unmodified) Keldysh parameter.

The most notable feature of all the spectra shown in Figures 2−4 is the ATI-like peak structure that is clearly visible for all three alcohols. Individual peaks in all the spectra are separated from each other by the single photon energy (3.1 eV for 400 nm light, 1.55 eV for 800 nm light). The peaks arise from MPI of an electron from the highest occupied molecular orbital (HOMO) of each alcohol molecule, leaving an alcohol ion in its ground electronic state. For instance, in the case of ethanol (Figure 3), the minimum number of 400 nm wavelength photons necessary for ionization is 4. In addition to the 4-photon peak the spectrum in Figure 3 also reveals 5-, 6-, and 7-photon ATI-like peaks. Similar behavior is observed for the entire data set depicted in Figures 2−4. We note that the total ionization probability of the alcohols may most probably be attributed to removal of a lone-pair electron of the oxygen atom in each of the molecules as well as to a contribution from ionization of the alkyl group. The relative contributions from these two will be dependent on laser intensity, with the former process contribution most in the low-intensity regime.

For purposes of comparison with an atomic system, we depict in Figure 5 typical electron spectra of Xe that we measured using 800 and 400 nm light at values of peak laser intensity varied over the range 30−420 TW. Note that the ionization energy of Xe, 12.13 eV, is higher than those of linear alcohols, 10.85, 10.46, and 10.25 eV, for methanol, ethanol, and 1-propanol, respectively, and thus the laser intensity employed for Xe is higher than that for linear alcohols to cover a similar range of $\gamma$-values down to 0.8. For present purposes, we focus on the similarities and differences that are observed in the electron spectra we measured for each of the alcohols and Xe using 800 and 400 nm light.

**Atomic-Like Feature of 800 nm Spectra.** In all spectra of the three linear alcohols and Xe measured using 800 nm light, the clearly resolved ATI-like peaks give way to featureless spectra as $\gamma$ approaches unity, as has been previously noted.[36] The overall spectral features are remarkably similar for all three linear alcohols and Xe.

One must take cognizance of an important and inevitable experimental feature that contributes to the continuous nature of the electron energy distribution, namely the inevitable focal volume effect that gives rise to three-dimensional spatial averaging of laser intensity over the laser focal volume. Thus, purely spatial aspects of the focal volume that is sampled by the TOF spectrometer will be expected give rise to the "washing out" effect on sharply structured peaks in the electron energy distribution. The temporal aspects associated with the laser pulse also contribute to the "washing out" effect: as the laser intensity changes in the course of the laser pulse, it gives rise to an associated temporal variation of $U_p$ that, in turn, makes the positions of ATI-like peaks vary in the course of the laser pulse. The loss of peak resolution due to this "washing out" depends purely on $U_p$ and the peak separation that is given by the energy

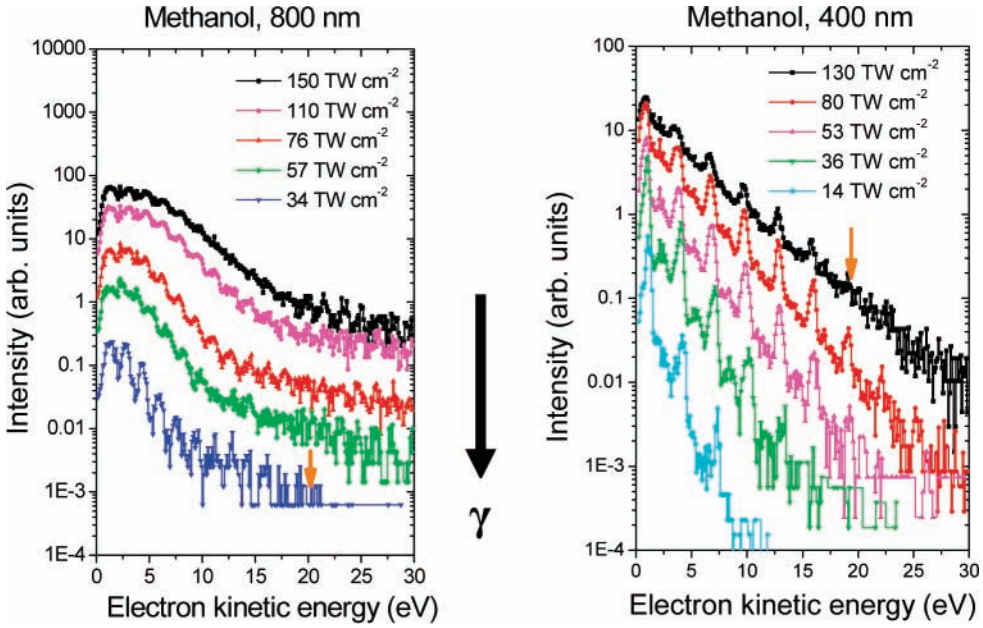


**Figure 2.** Electron spectra of methanol measured using 800 and 400 nm light at different intensities. Note the well-resolved structure due to above-threshold ionization that is visible at all intensities at 400 nm and at the lower intensities at 800 nm. The vertical arrows indicate the energy corresponding to $10U_p$ at an intensity of 130 TW cm$^{-2}$ (see text).

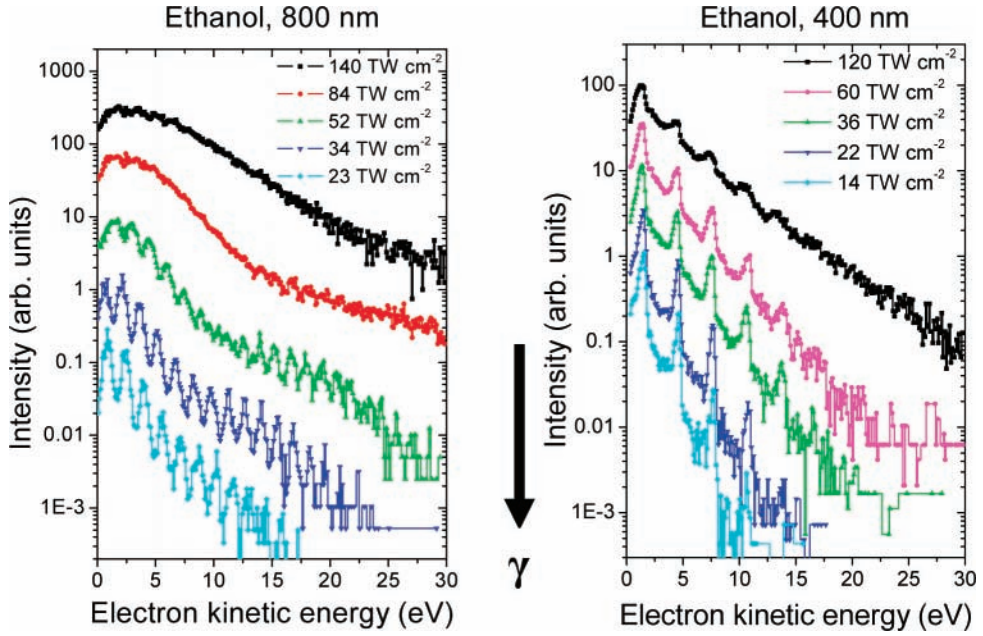


**Figure 3.** Electron spectra of ethanol measured using 800 and 400 nm light at different intensities. Note the well-resolved structure due to above-threshold ionization that is visible at almost all intensities at 400 nm and at the lower intensities at 800 nm.

of a single photon, $U_p > h\nu$, and has nothing to do with the ionization energy of the molecule and, thus, the ionization dynamics characterized by the adiabaticity ($\gamma$) value.

The observed gradual disappearance of sharp peaks in the spectra of linear alcohols and Xe at 800 nm laser light, however, occurs at similar values of $\gamma$ rather than at similar laser intensity, in spite of the difference in the ionization energy between linear alcohols and Xe. Therefore, the observed loss of sharp peaks seems to be beyond the above-described "washing out" effect and may be attributed to other facets that are of relevance to the overall ionization dynamics.

We suggest that the transition from structured electron spectrum into a featureless one might be regarded an indicator of the transition from the MPI regime to the tunnel ionization regime. Then the observed "washing out" effect with increasing $\gamma$ seems to validate the rationale for the present experimental study that the overall morphology of electron spectra provides a relatively unambiguous signature of the ionization regime that is being accessed for a given set of experimental conditions (like laser wavelength, peak laser intensity, and the zero-field ionization energy of the irradiated species). Referring to the resemblance of the electron spectra between three linear molecules and Xe at similar values of $\gamma$, we conclude that the linear alcohols exhibit atom-like properties as far as ionization dynamics in strong optical fields are concerned, i.e., those relying on the KFR-ADK model. It is important to reiterate at this stage that our present measurements do not allow us to comment on ionization probabilities in quantitative terms.

**Molecular Feature of 400 nm Spectra.** We now focus on the spectra that we measured using 400 nm radiation. Here, the

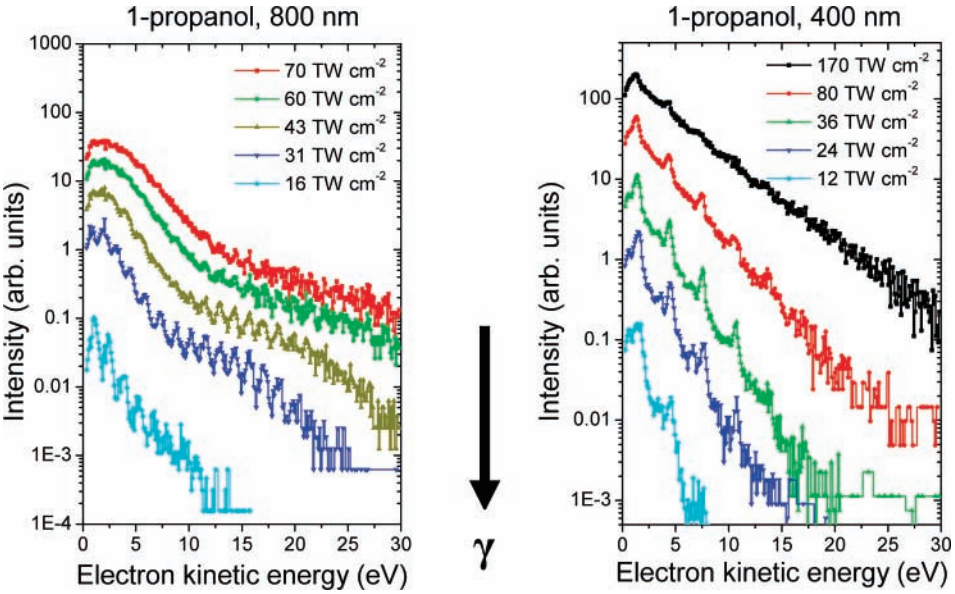


**Figure 4.** Electron spectra of 1-propanol measured using 800 and 400 nm light at different intensities. Note the well-resolved structure due to above-threshold ionization that is visible at almost all intensities at 400 nm and at the lower intensities at 800 nm.

**TABLE 1: Computations of Conventional and Modified Values of the Adiabaticity Parameter, $\gamma$, for Irradiation of Methanol, Ethanol, and 1-Propanol by 400 and 800 nm Laser Pulses at Peak Intensities, $I_{peak}$[a]**

| | | $\gamma$ | | |
|---|---|---|---|---|
| | $I_{peak}$ ($10^{13}$ W cm$^{-2}$) | conventional | MO-based | structure-based |
| methanol | 1.4 | 5.3 | 4.0 | 3.4 |
| 400 nm | 3.6 | 3.2 | 1.7 | 0.7 |
| | 5.3 | 2.6 | 1.0 | OBI |
| | 8.0 | 2.1 | OBI | OBI |
| | 13.0 | 1.7 | OBI | OBI |
| methanol | 3.4 | 1.6 | 0.9 | 0.4 |
| 800 nm | 5.7 | 1.3 | 0.4 | OBI |
| | 7.6 | 1.1 | OBI | OBI |
| | 11.0 | 0.9 | OBI | OBI |
| | 15.0 | 0.8 | OBI | OBI |
| ethanol | 1.4 | 5.0 | 3.7 | 2.6 |
| 400 nm | 2.2 | 4.0 | 2.6 | 1.3 |
| | 3.6 | 3.1 | 1.6 | OBI |
| | 6.0 | 2.4 | 0.7 | OBI |
| | 12.0 | 1.7 | OBI | OBI |
| ethanol | 2.3 | 2.0 | 1.3 | 0.6 |
| 800 nm | 3.4 | 1.6 | 0.9 | OBI |
| | 5.3 | 1.3 | 0.5 | OBI |
| | 8.4 | 1.0 | OBI | OBI |
| | 14.0 | 0.8 | OBI | OBI |
| propanol | 1.2 | 5.4 | 4.0 | 3.1 |
| 400 nm | 2.4 | 3.8 | 2.3 | 1.3 |
| | 3.6 | 3.1 | 1.5 | OBI |
| | 8.0 | 2.1 | OBI | OBI |
| | 17.0 | 1.4 | OBI | OBI |
| propanol | 1.6 | 2.3 | 1.6 | 1.2 |
| 800 nm | 3.1 | 1.7 | 0.9 | 0.3 |
| | 4.3 | 1.4 | 0.6 | OBI |
| | 6.0 | 1.2 | 0.3 | OBI |
| | 7.0 | 1.1 | OBI | OBI |

[a] Conventional $\gamma$-values are deduced using the KFR model for atomic ionization; MO-based and structure-based $\gamma$-values have been deduced using *ab initio* quantum chemical methods (see text). OBI: over-the-barrier ionization.

energy of a single photon is doubled compared to the 800 nm radiation and the condition $U_p < h\nu$ is satisfied even at the highest laser intensity in Figures 2−4. The situation appears to alter. Indeed, in Figures 2−4, some semblance of ATI-like structure persists at the highest $\gamma$-values of 1.7−1.4 (see Table 1). However, the continuous baseline contribution appears to be significantly enhanced in the spectra of linear alcohols with the increase in the laser intensity. This continuous baseline contribution is much larger than that in the Xe spectra in Figure 5, not only at similar laser intensity but also at similar $\gamma$-values. Furthermore, the baseline contribution appears to be increased as one goes from methanol to 1-propanol.

We attempt to disentangle the two contributions, continuous baseline contribution and ATI-like peak contribution, by replotting, in Figure 6, electron energy spectra that we measured for the three alcohols, focusing on the lower energy portion. It immediately becomes clear that, quite expectedly, the competition between continuous baseline and peak contributions is dependent on electron energy. For instance, in the 6-photon case, the continuous baseline makes a significantly smaller contribution to the ionization. In contrast, Figure 6 also shows that the 4-photon peak rides on a continuous baseline, and this becomes more pronounced as the alcohol size increases from methanol to 1-propanol. This kind of molecular-size-dependent spectral features cannot be rationalized within the framework of the adiabaticity parameter based on the original Keldysh−Faisal−Reiss model of atomic ionization as we will discuss later.

We note here that in both methanol and ethanol spectra in Figure 6, distinct peaks are observed that can be readily rationalized, on energy conservation grounds, in terms of the resulting alcohol ion being in the ground electronic state (denoted X in the figure). However, the spectrum of 1-propanol in Figure 6 indicates not only ATI-like peaks that belong to the ionic ground electronic state but also some additional, weaker peaks that have to be ascribed to the first electronically exited state of the propanol ion. We note also that, at least in the case of ethanol, photoionization to the first electronically excited-state of the ion is energetically possible, but no signal corresponding to it was observed in our measurements.

**On Length-Dependent Adiabaticity.** We return to considering the relative contribution that the continuous featureless baseline of spectrum makes to the overall morphology. Figure 6 makes it obvious that this contribution becomes stronger as one goes along the series methanol, ethanol, to 1-propanol. This observation might lead one to conclude that the laser intensity at which transition occurs from the MPI to the tunneling regime depends on the size of alcohol molecules. It, therefore, becomes necessary for us to re-examine the possible role that size-

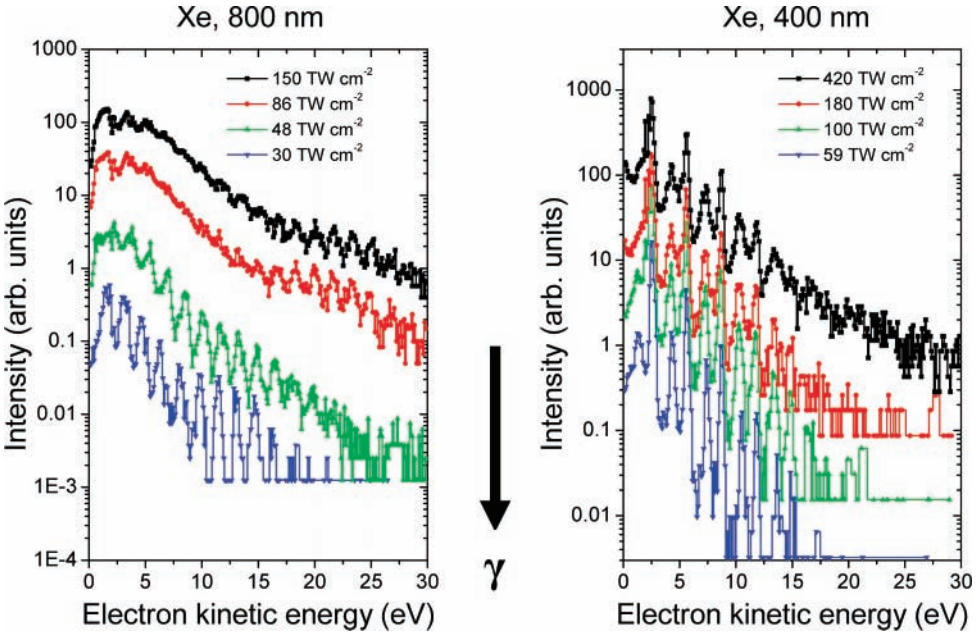


**Figure 5.** Electron spectra of Xe measured using 800 and 400 nm light at different intensities. Note the well-resolved structure due to above-threshold ionization that is visible at almost all intensities at 400 nm and at the lower intensities at 800 nm. In both panels the values of $\gamma$ increase, as indicated by the vertical arrow. For scaling we note that at 800 nm, $\gamma = 0.8$ for the topmost spectrum (150 TW cm$^{-2}$) and $\gamma = 1.8$ for the bottom-most spectrum (30 TW cm$^{-2}$).

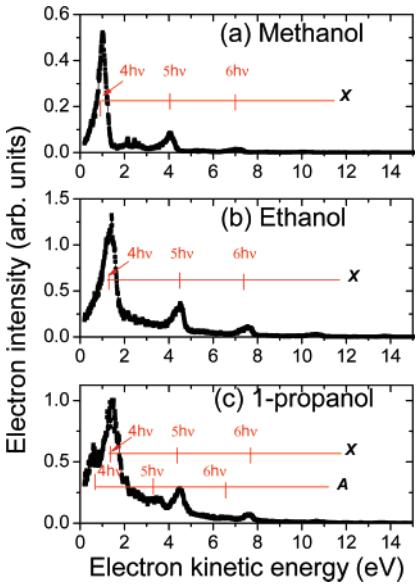


**Figure 6.** Energy spectra of low-energy electrons in methanol, ethanol, and 1-propanol, showing well-resolved structure attributable to 4-, 5-, and 6-photon ATI processes involving the ground electronic state, denoted X, of the molecular ion. Note the additional peaks that appear in the propanol spectrum that are attributed to denotes the 4- and 5-photon ATI processes involving the first excited electronic state, denoted A, of the molecular ion. All three spectra were measured using an intensity of 36 TW cm$^{-2}$, yielding $\gamma$-values of 3.2, 3.1, and 3.1 for methanol, ethanol, and 1-propanol, respectively.

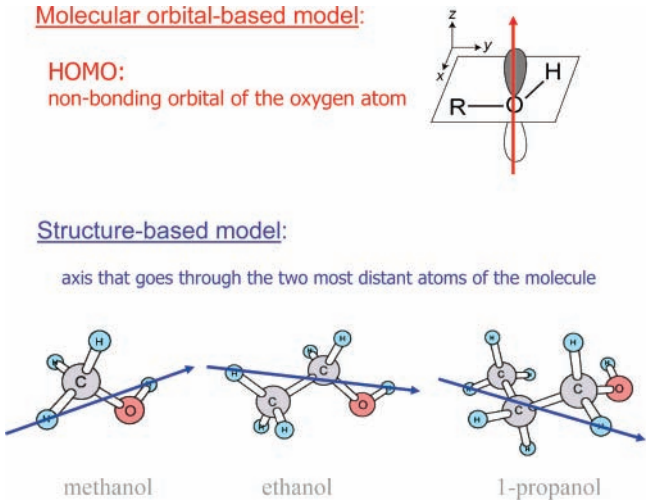


**Figure 7.** Schematic depiction of how computations were carried out on modifying the Keldysh parameter using molecular orbital considerations and molecular structure considerations (see text).

dependent (or length-dependent) $\gamma$ might play in the overall ionization dynamics in the linear alcohols.

To explore the possible utility of modified $\gamma$-values, where the modification might be molecular structure-based or molecular-orbital-based, we carried out the following *ab initio* quantum chemical computations. First, we carried out a geometry optimization of the structure of each of the neutral alcohol molecules using 6-311++G** basis sets. Then one-dimensional electrostatic potentials were calculated for the optimized geometry along (i) the nonbonding lone-pair orbital of the oxygen atom, which is the HOMO for the alcohol molecules and lies perpendicular to the molecular frame containing the C and O atoms in the molecular orbital-based model, and (ii) the axis between the most distant nuclei in the structure-based model. Figure 7 illustrates the two methods that we utilized in schematic form. We add the laser induced external field (assumed to be static) to the calculated one-dimensional electrostatic potential and estimate a barrier length $l_b$ in each case so that the length-modified adiabaticity parameter could be deduced. Our results, shown in Table 1, indicate that for methanol, ethanol, and 1-propanol, modified $\gamma$-values are difficult to reconcile with the morphology of the electron spectra (Figures 2−4) that we have measured. For instance, in the case of each of the alcohol molecules, modified $\gamma$-values at laser intensities in excess of $\sim 8 \times 10^{13}$ W cm$^{-2}$ indicate that electrons are formed via over-the-barrier ionization (or barrier suppression ionization). If this were the case, it would certainly not give rise to the type of spectra that we have actually measured in

our experiments. We have taken cognizance of saturation effects at higher laser intensities. Saturation can occur when over-the-barrier ionization sets in, and it can also occur due to normal focal volume effects wherein each and every molecule that is present in the focal volume is ionized by the incident optical field. The latter case is readily amenable to experimental probing: the electron and ion yields scale with incident laser intensity, $I$, as $I^{3/2}$ and this, indeed, appears to be case in spectra that we measured at the higher end of the intensity range we utilized in our experiments.

**Role of Electron Rescattering.** We discuss in the following possible effects of electron rescattering that may be responsible for the alteration in the morphology of the electron spectra as values of $\gamma$ change. As noted previously,[36] it is expected that atomic resonances and above-threshold ionization peaks would manifest themselves clearly in electron energy spectra in the MPI regime, whereas in the tunneling regime, the shape of the electron energy spectrum would be largely determined by its classical propagation in the optical field. This brings to the fore a special feature of strong-field ionization dynamics in the tunneling regime: electrons that are tunnel ionized from a molecule continue to "feel" the effect of the optical field even after the initial ionization event is over. The wavepacket that describes the ionized electron initially moves away from the vicinity of the parent molecule. However, when the incident laser light is linearly polarized, the electronic wavepacket is pulled back toward the parent molecule half a cycle after its initial formation.

The probability of recollision between the electron and the parent molecule depends on the laser phase as well as on the initial velocity and initial position of the electronic wave packet. Such rescattering allows the nuclear wavepacket to be probed with time resolutions that are lower than the pulse duration afforded by the laser that is used. Indeed, the correlation between the electronic and nuclear wavepackets that are created in tunnel ionization has been effectively utilized to probe the motion of the vibrational wavepacket of $D_2^+$ over several femtoseconds with remarkable temporal and spatial accuracy of 200 as and 0.05 Å, respectively.[37]

Although relatively little work has been carried out on electron rescattering on polyatomic molecules in general, experiments have been reported on how rescattering affects the ionization dynamics of linear alcohols[38] and other polyatomics[39] at peak intensities of $1 \times 10^{15}$ W cm$^{-2}$ and above, at wavelengths in the region of 800 nm, and the recently developed molecular **S**-matrix theory of Muth-Böhm et al.[24] explicitly takes rescattering into account.

The rescattering process may also, under appropriate conditions, contribute to "overwriting" the effect of the ATI-like peaks in electron spectra, giving rise to a smooth, featureless energy distribution, particularly as laser intensity values increase to allow for not just single ionization but also double (and multiple) ionization. There are physical reasons that can be invoked to rationalize this observation, as already noted in the context of atomic double ionization.[31] If the rescattering gives rise to ejection of a second electron, the excess energy will then be distributed among these two electrons in continuous fashion, "washing out" sharp features in the resulting electron energy spectrum that is measured.

Our latest electron-ion coincidence experiment on ethanol at 400 nm irradiation indeed revealed that the continuous baseline can mostly be attributed to multiple ionization events.[40] It is worth noting that the multiple ionization cannot be directly correlated to the direct ionization by the inelastic recollision, because the recollision energy ($<3.14U_p$) of the quiver electron is not necessarily higher than the ionization energy of the molecular ion, especially in the case of 400 nm irradiation. The rescattering, may, however, cause other inelastic processes, such as rovibrational excitation and electronic excitation. The inelastic rescattering may also take place on the ionic core that is electronically and vibronically excited. The final energy of the electron that one measures in an experiment such as ours is the result of a number of these factors. The increase in the continuous baseline contribution with the increase in the molecular size may, therefore, be attributed to the increase in the rates of inelastic rescattering that involves rovibrational and electronic excitation and sequential ionization.

**Electron Emission beyond $10U_p$.** It is necessary to make another observation with regard to one facet of the overall morphology of the electron spectra that we have measured. As indicated in some of the spectra that are depicted in Figures 2−4, electron energy values that we measured using 400 nm light appear to extend to regions beyond the energy corresponding to $10U_p$ for the highest laser intensities. Similar electron spectra of Xe (see Figure 5) and other rare gases using both 400 and 800 nm light do not exhibit extension of the high-energy tail above $10U_p$, as is expected on the basis of presently accepted wisdom.[41] The corresponding situation in some of the alcohols remains ambiguous at present and further work is clearly necessary.

## Summary

In summary, we have made measurements of electron energy spectra to probe the ionization dynamics of methanol, ethanol, and 1-propalol upon irradiation by intense, femtosecond 800 and 400 nm light pulses. As for the spectra that we measured using 800 nm irradiation, we find that our results can be readily rationalized within the framework of the original adiabaticity parameter based on the atomic KFR model: bifurcation between the multiphoton ionization and tunneling ionization regimes is accomplished on the basis of measured electron energy spectra without recourse to any structure-dependent modifications to the adiabaticity parameter. In that sense, the linear alcohols that we have experimentally probed appear to exhibit atom-like properties. Quite counterintuitively, strong-field ionization of linear alcohol molecules by the 800 nm laser pulses appears to be adequately described within the framework of an atom ionization model that utilizes a zero-range potential and yields atom-like adiabaticity parameters, $\gamma$. We note that although other $\gamma$-values that are listed in Table 1 are not incorrect *per se*, our results allow us to offer the conjecture that it appears not to be necessary to invoke these length-corrected or molecular orbital modified $\gamma$-values.

We also made use of 400 nm photons to illustrate the limitations of a purely atom-like picture of strong-field ionization, and our results show that purely molecular effects, like the possibility of inelastic electron scattering leading to rovibrational excitation, also influence the ionization dynamics.

## References and Notes

(1) Bandrauk, A. D. *Molecules in Laser Fields*; Dekker: New York, 1994.

(2) Hering, Ph.; Cornaggia, C. *Phys. Rev. A* **1999**, *59*, 2836.

(3) Bhardwaj, V. R.; Rayner, D. M.; Villeneuve, D. M.; Corkum, P. B. *Phys. Rev. Lett.* **2001**, *87*, 253003.

(4) Harada, H.; Tanaka, M.; Murakami, M.; Shimizu, S.; Yatsuhashi, T.; Nakashima, N.; Sakabe, S.; Izawa, S.; Tojo, S.; Majima, T. *J. Phys. Chem. A* **2003**, *107*, 6580.

(5) Kono, H.; Nakai, K.; Kanno, M.; Sato, Y.; Koseki, S.; Kato, T.; Fujimura, Y. In *Progress in Ultrafast Intense Laser Science*; Yamanouchi,

K., Chin, S. L., Agostini, P., Ferrante G., Eds.; Springer: Berlin, 2007; Vol. 3, in press.

(6) Bandrauk, A. D.; Kono, H. *Advances in Multi-Photon Processes and Spectroscopy*; Lin, S. H., Villaeys, A. A., Fujimura, Y., Eds.; World Scientific: Singapore, 2003; Vol. 15, p 147.

(7) Wang, S.; Tang, X.; Gao, L.; Elshakre, M. E.; Kong, F. *J. Phys. Chem. A* **2003**, *107*, 6123.

(8) Huang, J.; Wu, C.; Xu, N.; Liang, Q.; Wu, Z.; Yang, H.; Gong, Q. *J. Phys. Chem. A* **2006**, *110*, 10179.

(9) Yatsuhashi, T.; Obayashi, T.; Tanaka, M.; Murakami, M.; Nakashima, N. *J. Phys. Chem. A* **2006**, *110*, 7763.

(10) Rajgara, F. A.; Mathur, D.; Ramachandran, H. *Chem. Phys. Lett.* **2007**, *438*, 31.

(11) Mathur, D.; Rajgara, F. A. *J. Chem. Phys.* **2006**, *124*, 194308.

(12) Mathur, D.; Rajgara, F. A. *J. Chem. Phys.* **2004**, *120*, 5616.

(13) Krishnamurthy, M.; Mathur, D.; Rajgara, F. A. *J. Chem. Phys.* **2004**, *121*, 9765.

(14) Volkov, D. M. *Z. Phys.* **1935**, *94*, 250.

(15) Sengupta, N. D. *Bull. Math. Soc.* (*Calcutta*) **1952**, *44*, 175.

(16) Vachaspati. *Phys. Rev.* **1962**, *128*, 664.

(17) Fried, Z. *Phys. Lett.* **1963**, *3*, 349.

(18) Nishishov, A. I.; Ritus, V. I. *Sov. Phys. JETP* **1964**, *19*, 529.

(19) Reiss, H. R. *J. Math. Phys.* **1962**, *3*, 59.

(20) Keldysh, L. V. *Sov. Phys. JETP* **1965**, *20*, 1307.

(21) Faisal, F. H. M. *J. Phys. B* **1973**, *6*, L89.

(22) Reiss, H. R. *Phys. Rev. A* **1980**, *22*, 1786.

(23) Krainov, V. P. *J. Opt. Soc. Am. B* **1997**, *14*, 425.

(24) Ammosov, M. V.; Delone, N. B.; Krainov, V. P. *Sov. Phys. JETP* **1986**, *64*, 1191.

(25) Muth-Böhm, J.; Becker, A.; Chin, S. L.; Faisal, F. H. M. *Chem. Phys. Lett.* **2001**, *337*, 313.

(26) Zhao, Z. X.; Tong, X. M.; Lin, C. D. *Phys. Rev. A* **2003**, *67*, 043404.

(27) Walsh, T. D. G.; Ilkov, F. A.; Decker, J. E.; Chin, S. L. *J. Phys. B* **1994**, *27*, 3767.

(28) Litvinyuk, I. V.; Lee, K. F.; Dooley, P. W.; Rayner, D. M.; Villeneuve, D. M.; Corkum, P. B. *Phys. Rev. Lett.* **2003**, *90*, 233003.

(29) Yatsuhashi, T.; Obayashi, T.; Tanaka, M.; Murakami, M.; Nakashima, N. *J. Phys. Chem. A* **2006**, *110*, 7763.

(30) Kjeldsen, T. K.; Bisgaard, C. Z.; Madsen, L. B.; Stapelfeldt, H. *Phys. Rev. A* **2003**, *68*, 063407.

(31) DeWitt, M. J.; Levis, R. J. *J. Chem. Phys.* **1998**, *108*, 7739.

(32) Chaloupka, J. L.; Rudati, J.; Lafon, R.; Agostini, P.; Kulander, K. C.; DiMauro, L. F. *Phys. Rev. Lett.* **2003**, *90*, 033002.

(33) Hankin, S. M.; Villeneuve, D. M.; Corkum, P. B.; Rayner, D. M. *Phys. Rev. A* **2001**, *64*, 013405.

(34) Lezius, M.; Blanchet, V.; Ivanov, M. Yu.; Stolow, A. *J. Chem. Phys.* **2002**, *117*, 1575.

(35) Freeman, R. R.; McIlrath, T. J.; Bucksbaum, P. H.; Bashkansky, M. *Phys. Rev. Lett.* **1986**, *57*, 3156.

(36) Hatamoto, T.; Okunishi, M.; Lischke, T.; Prümper, G.; Shimada, K.; Mathur, D.; Ueda, K. *Chem. Phys. Lett.* **2007**, *439*, 296.

(37) Talebpour, M.; Chien, C. Y.; Liang, Y.; Larochelle, S.; Chin, S. L. *J. Phys. B.* **1997**, *30*, 1721.

(38) Niikura, H.; Legare, F.; Hasbani, R.; Ivanov, M. Yu.; Villeneuve, D. M.; Corkum, P. B. *Nature* (*London*) **2003**, *421*, 826.

(39) Rajgara, F. A.; Krishnamurthy, M.; Mathur, D. *J. Chem. Phys.* **2003**, *119*, 12224.

(40) Rajgara, F. A.; Krishnamurthy, M.; Mathur, D. *Phys. Rev. A* **2003**, *68*, 023407.

(41) Hatamoto, T.; Prümper, G.; Okunishi, M.; Mathur, D.; Ueda, K. *Phys. Rev. A.* **2007**, *75*, 061402(R).

(42) Paulus, G. G.; Nicklich, W.; Xu, H.; Lambropoulos, P.; Walther, H. *Phys. Rev. Lett.* **1994**, 2851.